ELSEVIER

Polymer 41 (2000) 1883–1891

polymer

A micro/macro constitutive model for the small-deformation behavior of polyethylene

S. Nikolov, I. Doghri*

Université catholique de Louvain, Centre for Systems Engineering and Applied Mechanics (CESAME), 4 Av. G. Lemaitre, B-1348 Louvain-la-Neuve, Belgium

Received 3 November 1998; received in revised form 29 March 1999; accepted 5 May 1999

Abstract

A micromechanically-based constitutive model for high density polyethylene (HDPE) in small deformations is presented. The microstructure of HDPE consists of closely packed crystalline lamellae separated by layers of amorphous polymer. Here a semi-crystalline polymer is modeled as an aggregate of randomly oriented composite inclusions, each consisting of a stack of parallel lamellae with their adjacent amorphous layers. For the amorphous phase, the viscoelastic constitutive behavior is modeled, assuming a polydomain liquid-crystal-like structure and micromechanical parameters such as the elastic constant of distortion and the persistent length of polymer molecules are used. The viscoplastic behavior at yield is incorporated through the constitutive modeling of the crystalline lamellae. Constitutive equations for the composite inclusions are proposed and different homogenization schemes for the overall properties discussed. The intermediate phase linking the lamellae and the amorphous layers is assumed to form a surface layer around each lamella and its role in the yield behavior of HDPE is discussed.

Keywords: Polyethylene; Micromechanics; Homogenization

1. Introduction

Semi-crystalline polymers are now widely used as structural materials. At small strains they show strongly non-linear stress–strain behavior which depends on such characteristics as the overall crystallinity, the molecular weight, the molecular branch content, etc. Recently, some micro/macro constitutive models for semi-crystalline polymers have been elaborated [1,2]. These are the first successful steps towards understanding how the microstructural evolution during deformation influences the observed overall behavior of these materials. However, the modeling in Refs. [1,2] is restricted to finite strains, and important processes at microlevel (e.g. lamellar-to-fibrillar transition) are ignored.

In small deformations, it is very important to know how the microstructure determines the initial Young's modulus and the yield stress. An important feature of polymers is the dependence of the initial Young's modulus on the yield stress [3] which, to our knowledge, has not been explained yet from a micromechanical point of view. Viscoelasticity of semi-crystalline polymers is due to the amorphous phase behavior [4], which has not been explicitly modeled either. Rheological models do exist for the small deformation regime (e.g. Refs. [5,6]), but they cannot provide a clear link between the micro and macro scales.

In this paper, we develop a small-strain micro/macro model, which enables to simulate the macroscopic behavior of PE from physically based micromechanical modeling. In Section 2 we develop constitutive equations for a composite inclusion consisting of a stack of crystalline lamellae and their adjacent amorphous layers. The viscoelastic behavior of the amorphous phase is explained once the elastic distortion of the polymer molecules is assumed to be important. Viscoplasticity of the lamellae is modeled as in rate-dependent polycrystalline materials. It is assumed that the intermediate phase (linking the lamellae and the amorphous layers) forms a surface layer around each lamella. The influence of the intermediate phase on the yield behavior is also discussed.

The overall behavior of an aggregate consisting of lamellae stacks is considered in Section 3. Results and conclusions are presented in Sections 4 and 5.

The notation used is as follows: scalars are given in italics (γ), tensors are designated by bold-face symbols (**n**, **M**), the order of which is determined by the context. Tensor contractions over one or two indices are denoted by ($\cdot$) and (:), respectively. Tensor (dyadic) products are indicated by ($\otimes$).

* Corresponding author.

0032-3861/00/$ - see front matter
PII: S0032-3861(99)00330-4

Table 1
Slip systems and corresponding resistances for HDPE [2]

Slip system	$g^{(\alpha)}$ (MPa)
(100) [001]	8
(010) [001]	20
{110} [001]	20
(100) [010]	13.3
(010) [100]	20
$\{110\} > \langle 1\bar{1}0 \rangle$	17.6

2. Micromechanical constitutive modeling

2.1. Basic structural unit of polyethylene

The microstructure of PE can be modeled as a two-phase composite, consisting of flat crystalline lamellae separated by amorphous layers [2,4]. The lamellae of melt solidified PE are most often radially arranged in spherulitic structures, thus making the material macroscopically isotropic.

The PE crystals are formed by association and folding of long polymer molecules. They possess an orthorhombic symmetry with lattice parameters $a = 7.4$ Å, $b = 4.93$ Å and $c = 2.54$ Å. The main deformation mode in crystals is the crystallographic slip [4], which takes place on privileged planes (see Table 1).

Two deformation mechanisms of amorphous layers have been identified: interlamellar shear and interlamellar separation. Experiments show that interlamellar shear is the dominant deformation mode at small strains of PE [4]. Here, the interlamellar shear is taken into account with the choice of a basic structural unit consisting of a stack of parallel lamellae and their adjacent amorphous layers (Fig. 1). In Fig. 1, **n** denotes the normal unit vector to the lamellae surfaces, and **c** the unit vector of the direction of PE molecules in the crystals. Experimental observations show that the chain direction forms an angle with the normal vector ranging between 17 and 40° [2]. In our model $(\mathbf{n}, \mathbf{c}) = 30°$. For convenience when dealing with the overall behavior, we call a stack of lamellae and their adjacent amorphous layers *inclusion*. The crystalline phase content χ_c in each inclusion is considered to be equal to the overall crystallinity of the polymer.

PE is nearly an incompressible material (with Poisson's ratio, $\nu = 0.41$ [1]). Therefore, in order to have interlamellar separation in a given inclusion, there must be a flow of amorphous material into the interlamellar space, which would lead to microcavities. At small strains, no cavitation has been registered for PE and therefore this deformation mode should have negligible contribution to the overall strain. Consequently, the material is modeled as an aggregate of randomly oriented inclusions, which deform only by slip on well-defined planes. The spherulitic morphology is neglected because investigations have shown that the different morphologies have no influence on the mechanical properties [3].

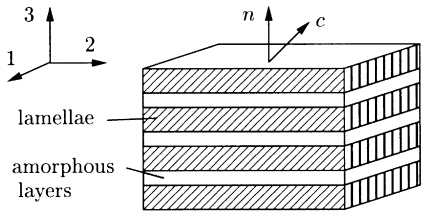

Fig. 1. Basic structural unit (inclusion) of PE.

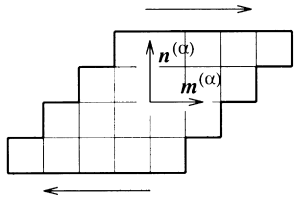

Fig. 2. Shear deformation of a single crystal.

It should be noted that a stack of lamellae can accomodate an arbitrary deformation, whereas a single polymer crystal cannot because polymer crystals are inextensible in a direction parallel to the polymer chains. Thus, our inclusion has five independent slip systems, which enable it to accomodate an arbitrary loading.

2.2. Crystalline phase

The deformation in polymer crystals can be described by the constitutive relations used for small-molecule crystals. For simplicity, we assume that the crystals are rigid-viscoplastic. In a single crystal the resolved shear stress $\tau^{(\alpha)}$ acting on a particular slip system (α) is given by the relation [7]:

$$\tau^{(\alpha)} = \boldsymbol{\sigma}_c : \mathbf{R}^{(\alpha)}, \tag{1}$$

where $\boldsymbol{\sigma}_c$ is the stress in the crystal and $\mathbf{R}^{(\alpha)}$ is the Schmid tensor attributed to the slip system (α):

$$\mathbf{R}^{(\alpha)} = \frac{1}{2}(\mathbf{n}^{(\alpha)} \otimes \mathbf{m}^{(\alpha)} + \mathbf{m}^{(\alpha)} \otimes \mathbf{n}^{(\alpha)}) \tag{2}$$

with $\mathbf{n}^{(\alpha)}$ and $\mathbf{m}^{(\alpha)}$ being the "slip plane" normal vector and the "slip direction" vector in this plane, respectively (Fig. 2).

For rate-dependent materials, the resolved shear stress $\tau^{(\alpha)}$ can be related to the corresponding shear rate $\dot{\gamma}^{(\alpha)}$ via a power law expression [7]:

$$\dot{\gamma}^{(\alpha)} = \dot{\gamma}_0 \text{sign}(\tau^{(\alpha)}) \left| \frac{\tau^{(\alpha)}}{g^{(\alpha)}} \right|^{1/m}, \tag{3}$$

where $\dot{\gamma}_0$ is a reference strain rate, $g^{(\alpha)}$ is the shear strength of the slip system (α) and m is the strain rate sensitivity.

Eq. (3) suggests that plastic flow is always present on the slip system (α) as long as the shear stress $\tau^{(\alpha)}$ is not identically equal to zero, but if $|\tau^{(\alpha)}| < g^{(\alpha)}$ the viscoplastic shear rate $\dot{\gamma}^{(\alpha)}$ is negligible.

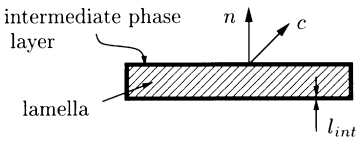

Fig. 3. Intermediate phase in PE.

The total strain rate in the crystal is:

$$\dot{\boldsymbol{\epsilon}}_c = \sum_{\alpha} \dot{\gamma}^{(\alpha)} \mathbf{R}^{(\alpha)}, \tag{4}$$

where the index α stands for the slip systems of PE crystallites. The slip systems and the corresponding resistances for HDPE crystals at room temperature are given in Table 1.

The slip resistances of polymer crystals depend on temperature, lamellar thickness and the normal stress acting on the slip planes [4,9,10]. As in Ref. [2], the strain-induced hardening of slip systems' strength is neglected because the thickness of lamellae (5–25 nm) suggests that dislocations must be quickly evacuated on lamellae surfaces.

The temperature dependence is easily understood as the crystallographic slip is a thermally activated process. As for the normal stress dependence, it has been established that the slip resistances are proportional to the applied normal stress, although the exact mechanism of this behavior is not clear [4].

There have been attempts to explain the yield behavior of PE as determined by the nucleation and propagation of screw dislocations along the chain axis **c** in the lamellae [8–10]. In the dislocation theory, the average lamellar thickness is directly related to the weakest resistance, $g^{(\alpha)}$ (thicker lamellae would have higher resistances $g^{(\alpha)}$). The theory gives reasonable results at room temperature but deviates significantly from the experiment at low temperatures and above the α-relaxation temperature (about 60°C). Our latest work supports the idea first suggested in Ref. [10], that the length of the Burgers vector along the axis decreases at higher temperatures.

We further consider the intermediate phase linking the lamellae and the amorphous layers (Fig. 3) and its role in the yield behavior of PE. The conformational entropy of a polymer system with homogeneous molecular structure and spatial inhomogeneity of density and orientation of polymer links has been treated in Ref. [11]. We make use of the basic results of Lifshitz (1969) on the entropy losses because of the spatial inhomogeneity in density and/or orientation which give rise to a density (orientation) gradient. Obvious sources of such a gradient in semi-crystalline polymers are the chain folding on lamellae surfaces where the chains bend more often in one direction than in other and the density difference between crystals and amorphous material. Thus, in semi-crystalline polymers each crystalline lamella should be wrapped with a surface layer (membrane) of intermediate phase.

The free energy of the intermediate layer, F_{int}, for a given lamella is a function of the density difference between two phases, Δn, the intermediate layer volume, V, and the thickness of the layer, l_{int}:

$$F_{\text{int}} = \frac{aTV\Delta n}{l_{\text{int}}^2}, \tag{5}$$

where T is the temperature, and a, the proportionality coefficient.

Assuming a membrane stress state in the intermediate layer, we can evaluate its surface tension σ as:

$$\sigma = F_{\text{int}}/V = \frac{aT\Delta n}{l_{\text{int}}^2}. \tag{6}$$

For more details see Ref. [11].

The intermediate phase volume fraction as measured from Mandelkern et al. [12] changes with crystallinity and we assume that it is directly related to the intermediate layer thickness. The results of these authors show that an increase in the overall crystallinity leads to decrease in the intermediate volume fraction and, therefore, surface tension will increase due to thinner intermediate layers. Here we suggest that the "failure" of the intermediate phase can explain the yield behavior at the second yield point where localized ("coarse") slip and, eventually, lamellar-to-fibrillar transition take place whereas the first yield point (which is more sensitive to crystallinity) can be explained with the help of dislocation theory. The role of intermediate phase in this case is to maintain homogeneous slip in the lamellae and prevent them from localization of deformation.

In conclusion, the introduction of the intermediate phase can explain the double yield phenomenon in HDPE reported by several authors (e.g. in Ref. [13]). At the first yield point, the intermediate phase prevents the lamellae from localization of deformation. The second yield point corresponds to the failure of the intermediate phase membrane.

2.3. Amorphous phase

The amorphous layers' microstructure is not fully understood at present, mainly because of the experimental difficulties stemming from the fact that it cannot be isolated and studied separately from the bulk material. A complex microstructure with ordered microdomains has been proposed in Ref. [15] in order to explain the large viscoplastic deformation of the amorphous phase of HDPE. Here we use a similar idea (though in a different context) in the case of small deformation behavior.

In the frame of our model, the relation between the shear viscosity and the shear rate in each inclusion can be extracted (at room temperature, the amorphous phase of PE is in a molten state, hence we use the shear viscosity as a key parameter). In Section 4 we show that it is of a power law type even at very small strain rates. This behavior is fundamentally different for PE melt where a Newtonian plateau is reached at small strain rates [16].

On the contrary, the polymer chains in the amorphous phase are subjected to severe constraints from the lamellae

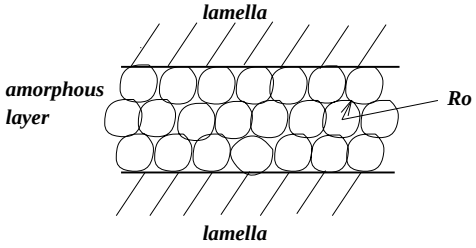

Fig. 4. Amorphous layers' microstructure.

and are situated in extremely thin layers with thickness of the order of 10 nm. We suggest that under these conditions, the viscoelastic stress in the amorphous layers is due to the resistance of polymer molecules to distortion during deformation. Micromechanical interpretations of viscoelasticity of homogeneous polymer melts speculate that stress is caused either by simultaneous stretching and release of polymer strands or reptation of polymer molecules in a "tube" of surrounding molecules [16]. These processes are not likely to operate in shearing of thin layers where most of the molecules are anchored in lamellae, chain ends are situated mostly on the lamellae surfaces [4] and entanglements are quite stable defects. We introduce a new parameter in the following, which reflects a different mechanism of viscoelasticity, i.e. the distortion elastic constant of molecules.

Our basic assumption is that each amorphous layer can be modeled as a polydomain structure (Fig. 4). Following Marrucci [17] and Wissbrun [18], it is assumed that each microdomain is in a local free energy minimum. The chain segments in a given microdomain do not have a net orientation prior to loading. According to the continuum theory of the nematics class of liquid crystals [19], the distortion free energy f_d of the chains per unit volume in a microdomain with radius R can be approximated by the following equation

$$f_d = K/R^2 \tag{7}$$

where K is the average elastic constant of distortion of a single microdomain. It is related to the distortion elasticity of polymer molecules and depends on their molecular structure and temperature.

When a shear rate $\dot{\gamma}_a$ is applied to the amorphous layer, the domains will change their radius from R_0 in the unloaded state to R in the steady state ($R_0 > R$), and the distortion energy in the layer will increase. From the conservation of volume, the number of microdomains grows as their radius diminishes. According to Marrucci [17], the increase of the distortion energy is equal to the steady state shear stress in the layer [18]:

$$\frac{K}{R^2} - \frac{K}{R_0^2} = \eta_a \dot{\gamma}_a, \tag{8}$$

where η_a is the layer's viscosity.

From these considerations, the domain radius in steady state shear, R, should depend on the applied shear rate $\dot{\gamma}_a$. In order to derive a relation between R_0, R and $\dot{\gamma}_a$ we introduce the probability for a microdomain, subjected to distant shear rate $\dot{\gamma}_a$, to have radius R as $P = R/R_0$ and require that in the *equilibrium state* $P|_{\dot{\gamma}_a=0} = 1$. Interaction between the microdomains is neglected. Then, according to statistical mechanics, P can be expressed as:

$$P = \exp\left(-\frac{W}{k_B T}\right), \tag{9}$$

where W is the energy (or work) necessary to shrink the microdomain to radius R, k_B is the Boltzmann constant and T the absolute temperature. We assume that W is a power law function of $\dot{\gamma}_a$ and Eq. (9) can be rewritten as:

$$R = R_0 \exp\left(-\frac{\alpha \dot{\gamma}_a^n}{k_B T}\right), \tag{10}$$

where $W = \alpha \dot{\gamma}_a^n$; n is the "shear rate sensitivity" of the microdomains and α is a proportionality constant.

Introducing Eq. (10) in (8) we obtain the shear viscosity of the amorphous phase as:

$$\eta_a = \frac{K}{(R_0)^2 \dot{\gamma}_a}\left[\exp\left(\frac{2\alpha \dot{\gamma}_a^n}{k_B T}\right) - 1\right]. \tag{11}$$

It is found numerically that the above equation is equivalent to a shear thinning power-law function ($\eta_a = C\dot{\gamma}_a^m$) up to very high strain rates, where a plateau of $\eta_a(\dot{\gamma}_a)$ is reached.

In addition to shrinking, the microdomains slide past each other. Wissbrun [18] derived the compliance modulus arising from mutual slip of two adjacent microdomains assuming a linear relation between the shear stress and strain. Similarly, we find the elastic modulus G_a resulting from microdomains' slip:

$$G_a = \frac{K}{RL} = \frac{K}{R_0 L}\exp\left(\frac{\alpha \dot{\gamma}_a^n}{k_B T}\right), \tag{12}$$

where L is the persistent length of the polymer molecule (the maximum chain length which can be considered as part of a straight line). Note that despite the assumption of a linear relation between shear stress and strain, G_a depends on $\dot{\gamma}_a$ through R.

In our viscoelastic modeling, it is assumed that upon shear, the microdomains' radius drops instantaneously from R_0 to R. The low energy required to shrink microdomains (see Section 4) suggests that this is a reasonable approximation. On the contrary, when deformation is suddenly frozen in a relaxation test, R will increase to its equilibrium value R_0 through thermal diffusion, but this process would take more time than shrinking upon external forces.

It is well known that two neighboring lamellae are linked up through numerous tie molecules passing from one lamella to another as well as through entangled chains anchored on lamellae surfaces [4]. Upon deformation the

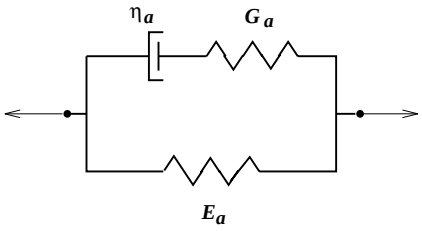

Fig. 5. Three-element rheological model for the amorphous phase behavior.

rubber-like stretching of the polymer molecules will produce elastic stress in the amorphous phase. At small strains, the entropic elasticity can be modeled by Neo-Hookean constitutive equations. As a result of the incompressibility, the only material parameter needed is the rubbery shear modulus E_a, which at microlevel is given as:

$$E_a = \nu_a k_B T \tag{13}$$

with ν_a being the number of the active polymer strands per unit volume.

So far we dealt with the parameters which should enter in the amorphous phase constitutive equations. In order to derive these equations we shall make some additional hypotheses backed by experimental results.

A viscoelastic constitutive model for the amorphous phase is developed based on the well-known three-element rheological model of Fig. 5 (it is shown in Ref. [6] that viscoelasticity of semi-crystalline polymers is well described by overstress theory, a slight modification of this model). Making the usual assumptions, the following differential equation relating the shear stress τ_a and strain γ_a acting on the amorphous phase is found to be:

$$\tau_a + \eta_a \frac{\partial}{\partial t}\left(\frac{\tau_a}{G_a}\right) = E_a \gamma_a + \eta_a\left[\dot{\gamma}_a + \frac{\partial}{\partial t}\left(\frac{E_a}{G_a}\gamma_a\right)\right], \tag{14}$$

where a superposed dot denotes a time derivative. If the coefficients E_a and G_a are constants, then Eq. (14) reduces to the three-element *linear* viscoelastic model:

$$\tau_a + \frac{\eta_a}{G_a}\dot{\tau}_a = E_a \gamma_a + \eta_a\left(1 + \frac{E_a}{G_a}\right)\dot{\gamma}_a. \tag{15}$$

However, the elastic modulus G_a is *not* a constant but depends on the strain rate $\dot{\gamma}_a$ according to Eq. (12); hence the differential equation in its general form (14) should be used. Unless the material is loaded with $\dot{\gamma}_a = constant$ from stress-and-strain-free state, Eq. (14) does not reduce to the linear case.

The multiaxial generalization of Eq. (14) is still under investigation. One could develop a 3D model along the same lines as the 1D model, and find the following differential equation relating the total stress and strain tensors ($\boldsymbol{\sigma}_a$ and $\boldsymbol{\epsilon}_a$) acting on the amorphous phase:

$$\boldsymbol{\sigma}_a + \mathbf{M} : \frac{\partial}{\partial t}(\mathbf{C}^{-1} : \boldsymbol{\sigma}_a) = \mathbf{E} : \boldsymbol{\epsilon}_a + \mathbf{M} : \left[\dot{\boldsymbol{\epsilon}}_a + \frac{\partial}{\partial t}(\mathbf{C}^{-1} : \mathbf{E} : \boldsymbol{\epsilon}_a)\right], \tag{16}$$

where $\mathbf{E}$ and $\mathbf{C}(I_2)$ are the fourth order stiffness tensors of the linear and non-linear elastic moduli, respectively, and $\mathbf{M}(I_2)$ is a fourth order tensor of the viscous moduli; I_2 is the second invariant of the strain rate tensor $\dot{\boldsymbol{\epsilon}}_a$.

Eq. (16) by itself does not translate the fact that at small strains the dominant mode of deformation of the amorphous layers is interlamellar shear. We can take this into account by another possible extension of the constitutive model from 1D to 3D as follows:

$$\dot{\boldsymbol{\epsilon}}_a = \dot{\gamma}_a \mathbf{R}_a, \tag{17}$$

where $\mathbf{R}_a$ is the Schmid tensor constructed from a pair of the lamellae normal vector $\mathbf{n}$ and the unit vector $\mathbf{m}^{(a)}$ along the projection of the stress vector in the inclusion on the lamellae surface:

$$\mathbf{m}^{(a)} = \frac{\mathbf{t}^{(a)}}{\|\mathbf{t}^{(a)}\|}; \quad \mathbf{t}^{(a)} = \boldsymbol{\sigma}\cdot\mathbf{n} - [(\boldsymbol{\sigma}\cdot\mathbf{n})\cdot\mathbf{n}]\mathbf{n}. \tag{18}$$

2.4. Constitutive equations of a single inclusion

The constitutive equations of the inclusion can be derived with the help of the assumption of uniform stress in it. This approximation is suitable for laminate composites subjected to off-plane shear. Let χ_c be the volume fraction of the crystalline phase, and χ_a the volume fraction of the amorphous layers. The total shear rate in the inclusion is then given by:

$$\dot{\boldsymbol{\epsilon}}_I = \chi_c \dot{\boldsymbol{\epsilon}}_c + \chi_a \dot{\boldsymbol{\epsilon}}_a \tag{19}$$

with $\dot{\boldsymbol{\epsilon}}_c$ given by Eq. (4) and $\dot{\boldsymbol{\epsilon}}_a$ obtained as discussed in Section 2.3.

3. Overall behavior

Once the constitutive behavior of a single inclusion is specified, we have to find the overall behavior of an aggregate consisting of randomly oriented similar inclusions. This can be done via a *homogenization* procedure and the results obtained will be an approximation of the macro. behavior of the material.

A *macro*. material point is viewed as the center of a representative volume element (RVE). If a macro. stress $\bar{\boldsymbol{\sigma}}$ is applied to the boundary of the RVE, then it can be shown that [21]:

$$\bar{\boldsymbol{\sigma}} = \langle \boldsymbol{\sigma}_I \rangle. \tag{20}$$

If a macro. strain $\bar{\boldsymbol{\epsilon}}$ is applied to the boundary of the RVE,

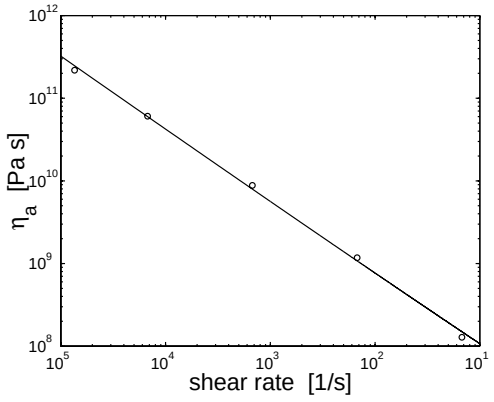

Fig. 6. Amorphous phase shear viscosity η_a vs. shear rate $\dot{\gamma}_a$.

then it is shown that [21]:

$$\bar{\boldsymbol{\epsilon}} = \langle \boldsymbol{\epsilon}_I \rangle. \tag{21}$$

The brackets $\langle\ \rangle$ denote volume averages over all inclusions.

The most widely used law describing the interaction between a single inclusion and the aggregate is known as the Voigt model in elasticity or the Taylor model in polycrystal metal plasticity.

This model suggests that in the aggregate, the strain within each inclusion is uniform and equal to the imposed macroscopic strain, i.e. Eq. (21) is trivially satisfied. In this approximation, the local compatibility between the inclusions is satisfied but the local traction equilibrium is not.

When the stress within each inclusion is assumed to be uniform and equal to the macroscopic stress (this is the Reuss model in elasticity or the Sachs model in plasticity), the local traction equilibrium between the inclusions is trivially satisfied but the local compatibility is violated.

Voigt (uniform strain) and Reuss (uniform stress) models give *upper* and *lower* bounds of the overall behavior, respectively. A more sophisticated model, which usually leads to more realistic predictions is the so-called self-consistent scheme. The basic assumption in self-consistent homogenization schemes is that the state of each inclusion in the aggregate is equivalent to that of the inclusion alone in a matrix (called homogeneous equivalent medium (HEM)) having the same stiffness $\bar{\mathbf{c}}$ as that -*unknown*- of the *whole aggregate*.

We are currently developing and implementing homogenization schemes for the constitutive model of Section 2. In our previous work we considered a fully viscoplastic model for each inclusion and used a self-consistent scheme to find the overall behavior (see Appendix). The results unveil that the Voigt model is not appropriate for semi-crystalline polymers and the reason for this is that the interaction between lamellae stacks is much weaker than that between the grains in metals. This conclusion is supported by the experimental evidence of freely rotating lamellae stacks during deformation [4], as well as by other results obtained by other authors [2]. Thus, the overall behavior of HDPE should be closer to the Reuss lower bound.

4. Results and discussion

The model was checked against uniaxial tensile experiments performed on INSTRON 4204 machine. The material is HDPE for gas pipes; the crystallinity χ_c measured by DEC has a value of $\chi_c = 0.67$. The standard tensile specimens have a width of 9.6 mm and a thickness of 3.95 mm in their thinner part. The initial gauge length is 50.5 mm, and the temperature is 23°C.

We first consider the strain rate dependence of the overall stress before yielding (at strain $\bar{\epsilon} = 0.08$) and its micromechanical interpretation. Five different macro-strain rates have been imposed on the specimens in tensile tests: $\dot{\bar{\epsilon}} = 6\times10^{-6}$; 3×10^{-5}; 3×10^{-4}; 3×10^{-3}; and $3\times10^{-2}\ \mathrm{s}^{-1}$. According to our model, the overall stress $\bar{\boldsymbol{\sigma}}$ splits into two parts:

$$\bar{\boldsymbol{\sigma}} = \bar{\boldsymbol{\sigma}}_v(\dot{\bar{\boldsymbol{\epsilon}}}, T) + \bar{\boldsymbol{\sigma}}_e(\bar{\boldsymbol{\epsilon}}, T) \tag{22}$$

where $\bar{\boldsymbol{\sigma}}_v(\dot{\bar{\boldsymbol{\epsilon}}}, T)$ is the rate-dependent, or viscous stress and $\bar{\boldsymbol{\sigma}}_e(\bar{\boldsymbol{\epsilon}}, T)$ is the elastic stress. They are both temperature-dependent but we leave the influence of temperature for further work.

Prior to yield, the rate-dependent contribution to the overall stress comes from the interlamellar shear in the randomly oriented inclusions. We first substract the reversible part of the overall stress $\bar{\boldsymbol{\sigma}}_e(\bar{\boldsymbol{\epsilon}})$ in Eq. (22) in order to obtain $\bar{\boldsymbol{\sigma}}_v(\dot{\bar{\boldsymbol{\epsilon}}})$: $\bar{\boldsymbol{\sigma}}_e(\bar{\boldsymbol{\epsilon}})$ is obtained via relaxation experiment as the stress after 24 h of relaxation at imposed strain of 8% ($\bar{\sigma}_e \approx 8$ MPa). We assume that the stress is uniform in all inclusions and consider the case of most unfavorable loading of the amorphous layers in a given inclusion, i.e. when the layers are oriented at 45° to the tensile axis. The rate-dependent part of the shear stress in the amorphous phase is then $\tau_a^{(v)} = \bar{\sigma}_v/2$.

In order to identify the parameter values in a first approximation, we assume that the strain rate is also uniform throughout the material and, *prior to yield*, the plastic strain rate is negligible. Then, for inclusions with amorphous layers inclined at 45° with respect to the tensile axis the average value of the shear rate is $\dot{\gamma}_I = 3\dot{\bar{\epsilon}}/4$. The shear rate in the amorphous phase will be $\dot{\gamma}_a \approx \dot{\gamma}_I/\chi_a$ (an important remark is that our model works not only in the reversible small-strain region but also *beyond* the yield limit of the material). We take $\chi_a \approx 1 - \chi_c = 0.33$.

At steady state shear the viscosity is given by

$$\eta_a = \frac{\tau_a^{(v)}}{\dot{\gamma}_a} \tag{23}$$

and we can convert the experimental "macro" stress–strain data in terms of viscosity vs. shear rate in the amorphous phase of a single inclusion (Fig. 6). It appears that the observed shear-thinning is of a power-law type and there

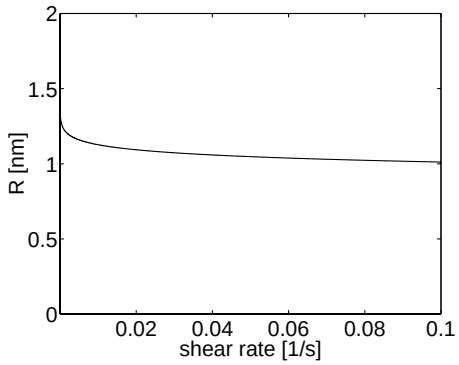

Fig. 7. Microdomain radius, R, vs. shear rate, $\dot{\gamma}_a$.

are no signs of Newtonian plateau for viscosity even for very small strain rates.

Some micromechanical parameters in our model cannot be directly measured despite their physical meaning. They can be fixed in a narrow range considering the restrictions imposed by the experimental evidence and physics. The average thickness of a single amorphous layer for HDPE is about 10 nm [3]. The hypothesis of a microdomain structure requires at least two microdomains over this thickness. We consider the initial microdomain radius to be $R_0 \approx 2$ nm.

On the contrary, the persistent length L for PE molecule is of the order of 1 nm [11]. The microdomain radius R cannot be smaller than this value at any strain rate because L is the smallest possible radius of curvature [18]. At high strain rates, R is controlled by the rate parameters α and n in Eq. (10). In addition, K has to be estimated before setting the values of α and n. For flexible molecules, K should be of the order of $10^{-11} \div 10^{-12}$ N [18] and n must be small in order to meet the requirement of minimum microdomain radius.

With these indications, we can proceed to a more precise parameter identification. We make use of shear thinning experimental results and numerical simulations with imposed simple shear on *a single inclusion*. The direction of shear is perpendicular to the lamellae normal **n** and the tensor components are with respect to the coordinate frame given in Fig. 1. This particular choice of the shear direction enables us to eliminate the plastic deformation prior to an imposed shear value of 0.1, and thus to obtain indicative results for the macroscopic behavior. The slip resistances of crystalline phase are taken from Table 1. After tuning, the following set of parameters is obtained: $R_0 = 1.8$ nm; $n = 0.1$; $K = 1.6 \times 10^{-11}$ N; $\alpha = 2.9 \times 10^{-21}$ J s^n; $T = 296$ K; $k_B = 1.38 \times 10^{-23}$ J K^{-1}, $L = 0.5$ nm, $E_a = 2$ MPa.

With these values, the shear thinning of amorphous phase is compared to the experimental data in Fig. 6. The evolution of microdomain's radius with strain rate is shown in Fig. 7. The stress–strain curves for a single inclusion subjected to simple shear (with $\chi_c = 0.67$) at three different strain rates are plotted in Fig. 8. The initial shear modulus does not change when different shear rates are applied which is due to the elastic stress in the amorphous layers. However, the yield stress diminishes with strain rate as observed in macroscopic experiments.

Our earlier results (see Appendix) have shown that the shape and relationship between different stress–strain curves obtained in simple shear for a single inclusion are homothetic to the macroscopic ones when a tensile experiment is performed. In this case, the initial shear modulus of a single inclusion corresponds to the macroscopic initial Young modulus and the inclusions' yield stress in shear is related to the macroscopic yield stress in tension.

We also performed simulations by changing the overall crystallinity χ_c in the inclusion (Fig. 9). The imposed shear rate is $\dot{\epsilon}_{I(13)} = 0.001$ s^{-1}. The weakest slip system resistances for different crystallinities ($\chi_c = 0.67, 0.55, 0.43$) are taken to be 8, 6.5, 5 MPa, respectively. The other slip resistances have been proportionally related to the weakest ones for each crystallinity level. From Fig. 9 it is seen that both the initial shear modulus and the shear yield stress decrease with decreasing crystallinity. The results obtained are very similar to those obtained in macroscopic tensile experiments. The relationship $g^{(\alpha)}/\chi_c = constant$ is imposed a priori but what is more important is that the link between the initial shear modulus and the yield stress is obtained as a direct result of our constitutive modeling keeping all the parameters of the amorphous phase model unchanged.

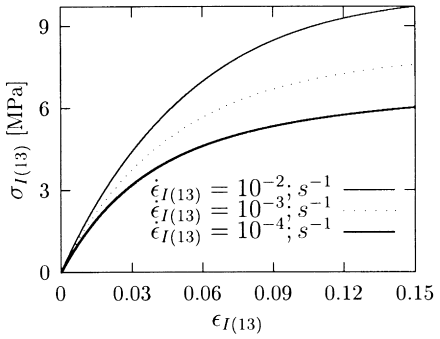

Fig. 8. Strain-rate dependence of inclusion's shear stress.

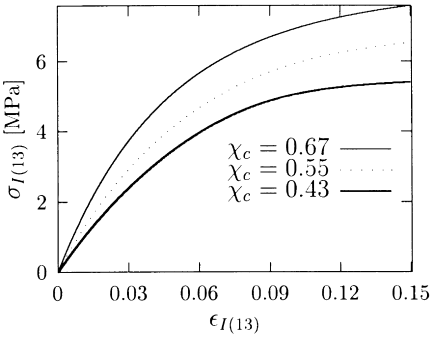

Fig. 9. Inclusion's shear stress as a function of crystallinity, χ_c.

The model allows us to compute the energy, W_a, necessary to shrink a microdomain to radius R. With the above parameter set, we obtain $W_a \approx 2 \times 10^{-21}$ J at strain rate, $\dot{\gamma}_a = 0.005\ s^{-1}$. At a first glance it seems to be excessively low. However, the energy necessary to move a dislocation in a PE crystal in order to set up plastic flow is about 1.6×10^{-19} J [4]. Therefore, the proposed mechanism of microdomains' shrinking should be active well before the propagation of dislocations in crystals.

Next, we consider the elastic contribution to the overall stress, $\bar{\boldsymbol{\sigma}}_e$. The rubbery shear modulus obtained from numerical simulations is $E_a = 2$ MPa, which gives the number of the active strands per unit volume to be $\nu_a = 0.5 \times 10^{27}\ m^{-3}$. A more representative estimation is to find the number of crystal's unit cells which can occupy the volume necessary for one strand to be formed. Simple computation suggests that one strand occupies a volume where 20 unit cells can be situated, which is a reasonable value (a small number of cells implies that the strand's conformation is near crystalline state and cannot be stretched much further which is in contradiction with the experimental evidence).

The results obtained for a single inclusion should be considered as a proof of the physical relevance of the proposed model. When micro/macro computer simulations are run (this is a work in progress), minor changes in the parameter values are possible.

5. Conclusions

The model we presented in this paper explains the stress–strain behavior of HDPE at small strains from a micromechanical point of view. It is valid in the temperature range where the amorphous phase state is above its glass transition temperature and the crystallinity level is high enough so that the notion of *amorphous layer* makes sense. It can be used for other semi-crystalline polymers as long as these conditions are met.

The hypothesis of liquid-crystal-like state of the amorphous phase (where the distortion energy of macromolecules determines its viscoelasticity) suggests the existence of microdomains, which shrink as long as shear deformation is applied. This picture explains well the strain-rate dependence of HDPE. The proposed constitutive equations describe correctly the observed non-linear stress–strain behavior.

The viscoplastic deformation in the crystalline lamellae is also incorporated in the model, which extends its use beyond yield. The relation between the initial Young's modulus and the yield stress for HDPE is obtained as a result of our constitutive modeling. We introduce the concept of the intermediate phase acting as a membrane wrapping each lamella; it gives an interpretation of the double yield phenomenon reported for HDPE.

The model can be naturally generalized in order to consider the temperature and pressure effects.

Acknowledgements

The authors wish to thank Mrs A. Goldberg from Solvay Research Laboratories (Brussels) for providing experimental data and valuable references, Dr L. Zealouk for providing the numerical results of Figs. 8 and 9, Mr S. Munhoven (UCL) for his help in the preparation of this paper. S. Nikolov gratefully acknowledges the financial support from UCL through FDS and FSR grants.

Appendix A

In a previous work [14], we developed and implemented purely viscoplastic models for both the crystalline and amorphous phases where the viscoplastic strain rate in a given inclusion is given by:

$$\dot{\boldsymbol{\epsilon}}_I = \sum_{\alpha} \dot{\gamma}^{(\alpha)} \mathbf{R}^{(\alpha)} + \sum_{\beta} \dot{\gamma}^{(\beta)} \mathbf{R}^{(\beta)}, \tag{A.1}$$

where the index α stands for the slip systems of PE crystallites and β denotes the additionally introduced slip systems (with a common slip plane perpendicular to **n**) related to interlamellar shear of amorphous layers.

The strength $g^{(\beta)}$ of the slip systems related to amorphous layer deformation evolves from zero in undeformed state to some saturation value. The evolution law proposed for $g^{(\beta)}$ is:

$$\frac{dg^{(\beta)}}{d\epsilon} = h\left(1 - \frac{g^{(\beta)}}{g_s}\right), \tag{A.2}$$

where h controls the initial slope of $g^{(\beta)}(\epsilon)$ and g_s is the saturation value of $g^{(\beta)}$. ϵ represents the equivalent strain in the inclusion. At macrolevel, g_s controls the yield stress σ_y, whereas h determines the initial Young's modulus E.

The yield stress, σ_y, depends linearly on the overall crystallinity, χ_c [3]. For crystallinity obtained from density measurements, $\chi_a = 15 + 2.29\sigma_y^{nom}$ with σ_y^{nom} being the nominal yield stress. On the contrary, numerical simulations with our model allowed us to relate the true yield stress and maximal interlamellar stress g_s via $\sigma_y = 4.13 + 2.53 g_s$. Hence, the relation between crystallinity and g_s becomes:

$$\chi_c = 23.61 + 5.275 g_s \tag{A.3}$$

In the above relations, χ is expressed in per cent, σ_y, σ_y^{nom} and g_s are in MPa.

In order to obtain the overall behavior, we use a *tangent* self-consistent scheme developed in Ref. [20]. It is supposed that the non-linear behavior of HEM can be approximated by the following constitutive law (under imposed macro. strain rate $\bar{\dot{\boldsymbol{\epsilon}}}$):

$$\bar{\mathbf{S}} = \mathbf{L}^{tg} : \bar{\dot{\boldsymbol{\epsilon}}} + \mathbf{S}' \tag{A.4}$$

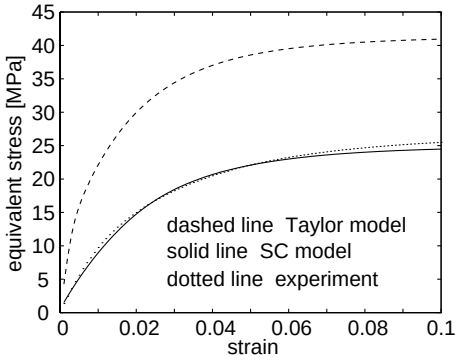

Fig. 10. Uniaxial tension of HDPE.

where $\bar{\mathbf{S}}$ is the deviatoric macroscopic stress, $\mathbf{L}^{tg}$ is the tensor of tangent viscoplastic moduli of HEM and $\mathbf{S}'$ is a "back stress" term, obtained in first order Taylor expansion of $\bar{\mathbf{S}} = f(\bar{\boldsymbol{\epsilon}})$. For each inclusion, the interaction law governing the deviation $(\dot{\boldsymbol{\epsilon}}_I - \dot{\bar{\boldsymbol{\epsilon}}})$, can be written in the form:

$$\mathbf{S}_I = \bar{\mathbf{S}} = [\mathbf{L}^{tg} + (\mathbf{R}^{tg})^{-1}] : (\dot{\boldsymbol{\epsilon}}_I - \dot{\bar{\boldsymbol{\epsilon}}}), \tag{A.5}$$

where $\mathbf{S}_I$ is the deviatoric stress within the inclusion, $\bar{\mathbf{S}}$ is the macroscopic deviatoric stress and the tensor $\mathbf{R}^{tg} = \mathbf{S}^0(\mathbf{L}^{tg})^{-1}$ accounts for the inclusion shape via the Eshelby tensor $\mathbf{S}^0$.

The micro/macro constitutive model was used to simulate a tensile test of HDPE for gas pipes at room temperature. The nominal strain rate is $\dot{\bar{\epsilon}}_{11} = 0.003s^{-1}$. The rate sensitivity is $m = 0.1$ [2]. The isotropic texture is approximated by 70 randomly oriented inclusions. The obtained stress–strain curves using Taylor and tangent self-consistent model are shown in Fig. 10.

References

[1] Dahoun A et al. Polym Engng Sci 1995;35:317.
[2] Lee BJ, Argon AS, Parks DM, Ahzi S, Bartczak Z. Polymer 1993;34:3555.
[3] Kennedy M, Peacock A, Mandelkern L. Macromolecules 1994; 27:5297.
[4] Lin L, Argon AS. J Mater Sci 1994;29:294.
[5] Kichenin J. PhD Thesis, Ecole Polytechn., Paris, 1992.
[6] Kitagava M, Zhou D. Polym Engng Sci 1995;35/22:1725.
[7] Asaro R, Needleman A. Acta Metall 1985;33:923.
[8] Shadrake LG, Guiu F. Phyl Magasine 1976;34:565.
[9] Young R. J Mater Forum 1988;11:210.
[10] Crist B, Fisher C, Howard P. Macromolecules 1989;22:1709.
[11] Grosberg AY, Khokhlov AR. Statistical physics of macromolecules. New York: American Institute of Physics, 1994.
[12] Mandelkern L, Alamo RG, Kennedy MA. Macromolecules 1990;23:4271.
[13] Lucas J, Failla M, Smith F, Mandelkern L. Polym Engng Sci 1995; 35/13:1117.
[14] Nikolov S, Doghri I. Micro/macro modeling and simulation of polyethylene in small strains. In: Proc 4th World Cong on Comp Mech, Buenos Aires, Argentina, 1998.
[15] Bartczak Z, Galeski A, Argon AS, Cohen R. Polymer 1996;37:2113.
[16] Larson R. Constitutive equations for polymer melts and solutions. London: Butterworth, 1988.
[17] Marrucci G. Int. Congr. Rheology, Acapulco, 1984.
[18] Wissbrun KF. Faraday Discuss Chem Soc 1985;79:161.
[19] de Gennes PG, Prost J. The physics of liquid crystals, 2. Oxford: Oxford University Press, 1993.
[20] Molinari A, Canova G, Ahzi S. Acta Metall 1987;35:2983.
[21] Nemat-Nasser S, Hori M. Micromechanics: overall properties of heterogeneous materials. Amsterdam: Elsevier, 1993.
[22] Lifshitz IM. Sov Phys JETP 1969;28:1280.